Efficiency Improvement of Wireless Power Transfer Based on Multitransmitter System

Zhaotian Yan, Bin Yang, Huan Liu, Changxin Chen, Muhammad Waqas, Ruikun Mai, *Senior Member, IEEE*, and Zhengyou He, *Senior Member, IEEE*

***Abstract*—Multitransmitter wireless power transfer system gets more and more applications as it can maintain high efficiency in a large space range. This article focuses on modeling the multi-transmitter system, and proposes an impedance matching method to improve efficiency under lateral-misalignment conditions. The theoretical analysis shows that the maximum transfer efficiency can be achieved as long as the equivalent input impedance of the transmitters is regulated to be the same under misalignment condition. Hence, a double closed-loop control strategy is proposed to realize maximum efficiency point tracking, where the primary control loop adjusts the input impedance of the transmitters through pulsewidth modulation, while the second control loop maintains constant output power by a dc–dc converter. A 500-W prototype is built to validate the feasibility of the proposed method. The efficiency is always higher than 90% with an improvement of up to 20.3% compared to that without such a method when the lateral misalignment increases from 0 to 10 cm (0%–41% of maximum coil size).**

***Index Terms*—DC–DC converter, efficiency, impedance matching, multitransmitter, wireless power transfer (WPT).**

I. Introduction

WIRELESS power transfer (WPT) is widely adopted as a simple and convenient charging method to get rid of twisted wire in many applications, such as vehicle [1], trains [2], biomedical implants [3], portable electronic and cellular mobile devices [4]. The efficiency, which is one of the most important parameters in the WPT system, should be improved as much as possible.

In a single-transmitter (TX) and single-receiver (RX) system, the efficiency is dynamically changing with the load conditions [5], the coupling coefficient [6], and quality factor [7]. In order to satisfy the requirements of efficiency, the research focuses on several directions, which are as follows.

Manuscript received November 4, 2019; revised January 16, 2020; accepted January 21, 2020. Date of publication February 3, 2020; date of current version May 1, 2020. This work was supported in part by the National Key Research and Development Program of China under Grant 2017YFB1201002, in part by the National Natural Science Foundation of China under Grant 51677155, and in part by the National Natural Science Foundation of China under Grant 51977184. Recommended for publication by Associate Editor J. Acero. *(Corresponding author: Ruikun Mai.)*

The authors are with the School of Electrical Engineering, Southwest Jiaotong University, Sichuan 611756, China (e-mail: zhaotian_yan@163.com; 546867343@qq.com; 2190581829@qq.com; 3166846659@qq.com; waqas.zeb@hotmail.com; mairk@swjtu.edu.cn; hezy@swjtu.edu.cn).

Color versions of one or more of the figures in this article are available online at https://ieeexplore.ieee.org.

Digital Object Identifier 10.1109/TPEL.2020.2971140

1) find the optimal operating frequency through automatic frequency tuning [8]–[10];
2) find the optimal load through impedance matching [11], [12];
3) uniform magnetic field by configuration of coils [13], [14].

However, when the relative position of the TX and the RX changes too much, such methods are very limited to the efficiency improvement because of the coupling coefficient's dramatic fluctuation [15]. Recently, researchers have paid much attention to the multi-TX WPT system because it can increase the effective charging range [16], [17], and the efficiency can be improved dramatically when the misalignment occurs [18]–[20].

To deliver power with high efficiency over a larger area in the multi-TX WPT system, Gosselin proposes a novel resonance based on the multi-TX structure [17], and the efficiency is increased dramatically through selecting the number of transmitters under different positions. In the field of portable consumer electronic products, a reconfigurable planar array of coupled-resonator coils is designed in [18] to charge a mobile receiver in three-dimensional space by choosing the optimal array configuration for a particular receiver position. Furthermore, a new single-layer winding array for planar wireless battery charging systems is presented in [16], which enables multiple devices to be placed and charged simultaneously on the wireless charging pad in a free-positioning manner.

Nevertheless, the uncertain position of the receiver results in an unknown coupling coefficient between RX and each TX during the charging period, which will decrease the transmission efficiency. Therefore, it is necessary to find the relationship between the system's efficiency and the mutual inductance so that maximum efficiency point tracking (MEPT) can be realized. Smith proposes a phased array method in the multi-TX system [21], and the relationship between the amplitude and phase of voltage in each TX and mutual inductance can be used to achieve the precise control of efficiency. In addition, researchers have drawn a conclusion that the current in each TX should be scaled proportionally to the ratio of coupling coefficients so that the MEPT can be achieved in the multi-TX system [22].

Therefore, researchers regulate the current in TXs according to the mutual inductance between each TX and RX, which is estimated by additional equipment, and the efficiency is improved dramatically [23], [24]. The empirical formula is used in [23] to predict mutual inductance by getting the system information

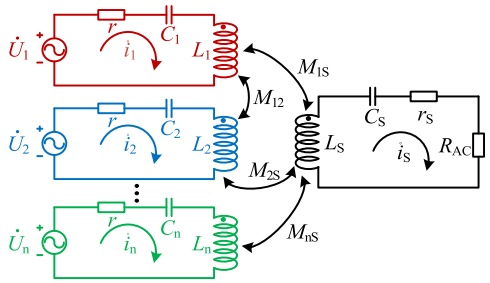

Fig. 1. Equivalent circuit model of multiple transmitters system.

on both TX and RX. In order to cancel the communication link, researchers give a good example of estimating mutual inductance while the value of the load on RX should be known beforehand. Besides, the estimation process is complex due to the high-frequency sampling and heavy computational burden [24]. In a word, it is of importance to avoid the mutual inductance estimating in the multi-TX WPT system.

This article investigates the theoretical analysis of the relationship between currents, voltages, and the mutual inductance of a multi-TX WPT system, where the couplings between each TX and RX are different. The impedance matching method is proposed implemented by adjusting the input impedance to allocate the transferred power between TXs and to improve efficiency when misalignment occurs. The maximum efficiency point has relationship to the RX load, the absolute strength of coupling, or the parasitic resistance of the coils so that the MEPT could be located without any the communication link between RX and TX.

The analysis of multi-TX systems is discussed in Section II. The topology and regulation are derived in Section III. Section IV gives the experimental results. Finally, the conclusion of the proposed approach is drawn in Section V.

II. Analysis of Multitransmitter System

The equivalent circuit with n number of transmitters and a single receiver is depicted in Fig. 1. The input voltage of each transmitter is $U_{\rm i}$, while $C_{\rm i}$, $L_{\rm i}$ and $C_{\rm S}$, $L_{\rm S}$ are the compensation capacitance and the self-inductances of the coil in the TX and RX, respectively. $M_{\rm iS}$ is the mutual inductance between $L_{\rm i}$ and $L_{\rm S}$, while $r_{\rm S}$ denotes the parasitic resistance in the RX. $R_{\rm AC}$ presents the equivalent ac load resistance of the rectifier.

The turns and size of each transmitting coil are set to be the same so that the parasitic resistance (r) and the self-inductance ($L_{\rm i}$) of each TX can be assumed to be identical ($1 \le i \le {\rm n}$).

As the system needs to be resonant, the relationship between inductors and capacitors in the system is described by the following equation:

$$\begin{cases} j\omega L_{\rm i} + \frac{1}{j\omega C_{\rm i}} = 0, \quad (1 \le i \le n) \\ j\omega L_{\rm S} + \frac{1}{j\omega C_{\rm S}} = 0 \end{cases} \tag{1}$$

According to Kirchhoff's voltage law (KVL), the matrix equation can be obtained as follows:

$$\begin{bmatrix} r & sM_{12} & sM_{13} & \cdots & sM_{1{\rm n}} & -sM_{1{\rm S}} \\ sM_{12} & r & sM_{23} & \cdots & sM_{2{\rm n}} & -sM_{2{\rm S}} \\ sM_{13} & sM_{23} & r & \cdots & sM_{3{\rm n}} & -sM_{3{\rm S}} \\ \vdots & \vdots & \vdots & \ddots & \vdots & \vdots \\ sM_{1{\rm n}} & sM_{2{\rm n}} & sM_{3{\rm n}} & \cdots & r & -sM_{{\rm nS}} \\ -sM_{1{\rm S}} & -sM_{2{\rm S}} & -sM_{3{\rm S}} & \cdots & -sM_{{\rm nS}} & r_{\rm S}+R_{\rm AC} \end{bmatrix} \begin{bmatrix} \dot{i}_1 \\ \dot{i}_2 \\ \dot{i}_3 \\ \vdots \\ \dot{i}_{\rm n} \\ \dot{i}_{\rm S} \end{bmatrix} = \begin{bmatrix} \dot{U}_1 \\ \dot{U}_2 \\ \dot{U}_3 \\ \vdots \\ \dot{U}_{\rm n} \\ 0 \end{bmatrix} \tag{2}$$

where $s = j\omega$ and ω denote the angular frequency of the system. Due to a WPT system with n transmitters, there might exist cross coupling in the system, which can make the analysis of the system somehow complicated. In order to minimize the effect of cross coupling and to simplify the analysis of the system, a bipolar pad (BPP) coil design, proposed in [25], is adopted here as the coupler. The coupler consists of two identical partially overlapped coils that are mutually decoupled. With this assumption, the cross-coupling would be small enough to be ignored. The resonant currents in TXs and RX can be derived according to the following equation:

$$\begin{cases} \dot{i}_m = \\ \frac{U_m \cdot \left[r \cdot (r_S + R_{\rm AC}) + \sum_{j=1, j\neq m}^{j=n} \omega^2 {M_{j{\rm S}}}^2\right] - \omega^2 M_{mS} \left(\sum_{j=1, j\neq m}^{j=n} U_j \cdot M_{jS}\right)}{r^2 \cdot (r_S + R_{\rm AC}) + \sum_{j=1}^{j=n} \omega^2 {M_{jS}}^2 \cdot r} \\ \dot{i}_S = \frac{\sum_{j=1}^{j=n} \omega \cdot M_{jS} \cdot U_j}{r \cdot (r_S + R_{\rm AC}) + \sum_{j=1}^{j=n} \omega^2 {M_{jS}}^2} \cdot 1i \quad (n \ge 1) \end{cases} \tag{3}$$

where $M_{\rm mk} = 0, 1 \le m \le n, 1 \le k \le n, m \ne k$.

The power transfer efficiency between transmitting coils and the receiving coil can be obtained as follows:

$$\eta = \frac{\dot{i}_S \cdot \bar{\dot{i}}_S \cdot R_{\rm AC}}{\dot{i}_S \cdot \bar{\dot{i}}_S \cdot (r_S + R_{\rm AC}) + \sum_{j=1}^{j=n} \dot{i}_j \cdot \bar{\dot{i}}_j \cdot r} \tag{4}$$

where $\bar{\dot{i}}_S$ and $\bar{\dot{i}}_j$ are the conjugation of $\dot{i}_S$ and $\dot{i}_j$, respectively.

The currents of transmitting coils can be regulated to the designed values to achieve MEPT. In this work, a strategy based on an impedance matching method is proposed to realize MEPT in a multiple-transmitter system. This approach is implemented by adjusting the input impedance to allocate the transferred power amongst TXs and to improve the efficiency when misalignment occurs. The current ratio $k_{\rm m}$ based on one of the branches can be presented as follows:

$$k_m = \frac{\dot{i}_m}{\dot{i}_1}, \quad (1 \le m \le n). \tag{5}$$

By substituting (5) into (4), we can obtain the efficiency as follows:

$$\eta = \frac{R_{\mathrm{AC}}}{(i_1/i_S)^2 \cdot (k_1^2 + k_2^2 + \cdots + k_n^2) \cdot r + r_S + R_{\mathrm{AC}}} \tag{6}$$

where i_m and i_S are the RMS value of $\dot{i}_m$ and $\dot{i}_S$, $(1 \le m \le n)$. According to KVL, the equation for RX current loop can be derived as follows:

$$i_S \cdot (r_S + R_L) - s \cdot M_{1S} \cdot i_1 - s \cdot M_{2S} \cdot i_2 - \cdots - s \cdot M_{nS} \cdot i_n = 0. \tag{7}$$

Substituting (5) and (7), the current ratio i_1/i_{S} is a function against $k_1, k_2, \ldots k_n$, which can be given as follows:

$$\frac{i_1}{i_{\mathrm{S}}} = g(k_1, k_2 \ldots k_n) = k_1 \cdot \frac{r_S + R_{\mathrm{AC}}}{k_1 \cdot s \cdot M_{1S} + k_2 \cdot s \cdot M_{2S} + \cdots + k_n \cdot s \cdot M_{nS}}. \tag{8}$$

Then, substituting (8) into (6), the power transfer efficiency could be simplified as follows:

$$\eta(k_1, k_2 \ldots k_n) = \frac{R_{\mathrm{AC}}}{g(k_1 \ldots k_n)^2 \cdot r \cdot (k_1^2 + k_2^2 + \cdots k_n^2) + r_S + R_{\mathrm{AC}}}. \tag{9}$$

To look for the maximum point of the *n*-variable function, the first-order partial derivative of $\eta\,(k_1, k_2, \ldots k_n)$ is set to be zero, which can be expressed as follows:

$$\frac{\partial \eta(k_1, k_2, \ldots, k_n)}{\partial k_{\mathrm{i}}} = 0, \quad (1 \le i \le n). \tag{10}$$

By simplifying the partial derivation, it can be transformed into

$$\frac{\partial}{\partial k_i}\left[\frac{\sum_{j=1}^{n} k_j^2}{\left(\sum_{j=1}^{n} (k_j \cdot M_{jS})\right)^2}\right] = 0, \quad (1 \le i \le n). \tag{11}$$

Therefore, the relationship between current and mutual inductance can be solved as follows:

$$k_i \cdot \sum_{j=1}^{n} k_j \cdot M_{jS} = M_{iS} \cdot \sum_{j=1}^{n} {k_j}^2, \quad (i = 1, 2, \ldots, n). \tag{12}$$

For simplification of the equation, the relationship between k_{i} and M_{iS} could be obtained by the following:

$$\frac{k_i}{k_{i+1}} = \frac{M_{iS}}{M_{(i+1)S}}, \quad (i = 1, 2, \ldots, n-1). \tag{13}$$

The final result is as follows:

$$i_1 : i_2 : \cdots : i_m = M_{1S} : M_{2S} : \cdots : M_{mS}, (1 \le m \le n) \tag{14}$$

which states that the current at TXs should be scaled according to the ratio of mutual inductance so that the efficiency can obtain the maximum value. For instance, if the coupling between TX2 and RX is half of that between TX1 and RX, the coil current at TX2 should be scaled to half. However, it is inconvenient to measure the mutual inductance to distribute the current of TXs. To solve this problem, the article will find the relationship between voltages in TXs. Then, by substituting (14) into (2), the voltages of the transmitters can be expressed as follows:

$$\begin{cases} U_1 = k_1 \cdot i_1 \cdot r - s \cdot k_1 \cdot M_{1S} \cdot i_S \\ U_2 = k_2 \cdot i_1 \cdot r - s \cdot k_2 \cdot M_{1S} \cdot i_S \\ \vdots \\ U_n = k_n \cdot i_1 \cdot r - s \cdot k_n \cdot M_{1S} \cdot i_S. \end{cases} \tag{15}$$

In summing up, it may be stated that the ratio of voltages and current in every TX is equal to the ratio of mutual inductance

$$U_1 : U_2 : \cdots U_n = i_1 : i_2 : \cdots i_n = M_{1S} : M_{2S} : \cdots M_{nS}. \tag{16}$$

In order to obtain the maximum efficiency, it may be stated that the ratio of voltage over current in every TX is equal to the ratio of mutual inductance between TXs and RX. The equivalent resistance of one TX can be defined as follows:

$$R_m = \frac{U_m}{i_m}, \quad (m = 1, 2, \ldots, n). \tag{17}$$

As a result, (16) can be converted into the following:

$$R_1 = R_2 = R_3 = \cdots = R_m, \quad (m = 1, 2, \ldots, n). \tag{18}$$

The efficiency will reach the maximum value if the equivalent resistances of TXs are the same. Furthermore, these criteria (18) do not relate to the RX load, the absolute strength of coupling or the parasitic resistance of the coils.

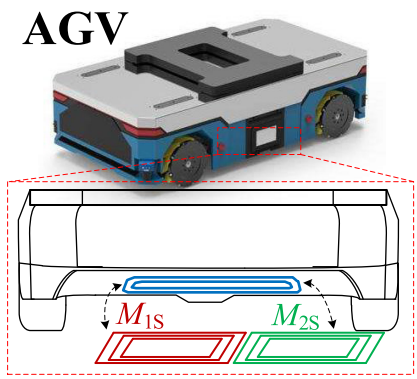

Fig. 2. Charging process of AGV.

III. Analysis of WPT System in Vehicle Charging

As shown in Fig. 2, it is inevitable that the transmitting coils are not aligned with the receiving coil during the charging process of automated guided vehicles (AGV) [27]. It is necessary to analyze such system, and discuss the efficiency, the power, and the control method to realize the MEPT.

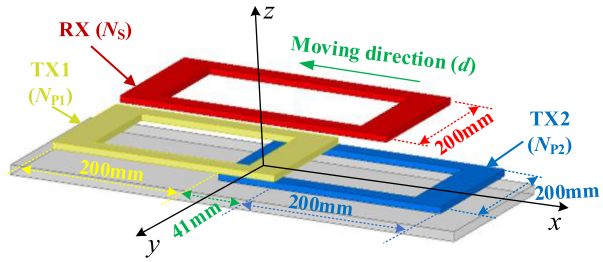

Fig. 3. Structure of the BBP coupling model in dual TXs WPT system.

A. Transfer Efficiency Analysis

According to (3), the loop currents can be obtained from the KVL equation if n is set to two

$$\begin{cases} \dot{i}_1 = \dfrac{\omega^2 \cdot M_{2S} \cdot (U_1 \cdot M_{2S} - U_2 \cdot M_{1S}) + U_1 \cdot r \cdot (r_S + R_{AC})}{r^2 \cdot (r_S + R_{AC}) + \omega^2 \cdot r \cdot \left({M_{1S}}^2 + {M_{2S}}^2\right)} \\ \dot{i}_2 = \dfrac{\omega^2 \cdot M_{1S} \cdot (U_2 \cdot M_{1S} - U_1 \cdot M_{2S}) + U_2 \cdot r \cdot (r_S + R_{AC})}{r^2 \cdot (r_S + R_{AC}) + \omega^2 \cdot r \cdot \left({M_{1S}}^2 + {M_{2S}}^2\right)} \\ \dot{i}_S = \dfrac{\omega \cdot (U_1 \cdot M_{1S} + U_2 \cdot M_{2S})}{r \cdot (r_S + R_{AC}) + \omega^2 \cdot \left({M_{1S}}^2 + {M_{2S}}^2\right)} \cdot 1i. \end{cases} \tag{19}$$

As a result, transfer efficiency (η) can be calculated

$$\eta = \frac{P_{out}}{P_{in}} = \frac{\dot{i}_S \cdot \bar{\dot{i}}_S \cdot R_{AC}}{\dot{i}_1 \cdot \bar{\dot{i}}_1 \cdot r + i_2 \cdot \bar{\dot{i}}_2 \cdot r + \dot{i}_S \cdot \bar{\dot{i}}_S \cdot (r_S + R_{AC})} \tag{20}$$

where P_{out} is the output power, and P_{in} is the input power. The research focuses on applying a BBP structured coil to dual TXs WPT system, which can eliminate the influence of mutual inductance between TXs [25]. The coupling model is presented in Fig. 3. The size of the receiving coil is reduced to fit the size of the AGV. The TX is covered with ferrite cores while the RX is not.

The coil size and moving direction are shown in Fig. 3. The extent of overlap between the two TXs is 41 mm, and the vertical distance between TXs and RX is 50 mm. N_{P1}, N_{P2}, and N_S are the turns of the transmitting coil 1, transmitting coil 2, and the receiving coil, respectively. The results can be obtained by simulation in ANSYS MAXWELL. When RX moves toward TX1 horizontally (d is the moving distance), M_{1S} increases, while M_{2S} decreases rapidly. In addition, M_{12} can be recognized to be equal to zero because it is mutually decoupled. The fluctuation of the self-inductance of the coil is small, which can be ignored.

According to (9), η has no relationship to the input voltage V_g, but it is a function against the horizontal misalignment (d) and the voltage ratio (k) among TXs. Meanwhile, the analytical solution of maximum efficiency is given by calculating the partial derivatives, when RX is at a certain position.

To analyze the characteristics of the system, the parameters of components are depicted in Table I.

The system's efficiency versus voltage ratio under the different ratios of mutual inductance is shown in Fig. 4. Such a method can maintain maximum efficiency with different misalignment scenarios by using the optimized voltage ratio.

At a certain misalignment, the efficiency of the system is related to k and the load R_{AC}. Fig. 5 shows the efficiency variation when the ratio of the mutual inductance (M_{1S}/M_{2S}) is equal to 0.5, and there exist an optimal load R_{AC} and k.

According to (18), the efficiency will get the maximum value when the equivalent impedance of each TXs are equal. Fig. 6(a) shows the maximum efficiency curve of dual-TX system, where

TABLE I
PARAMETERS OF FBDRT FOR SIMULATION

Description	Parameter
Input voltage (V_g)/V	110
Resonant frequency (f_s)/Hz	85000
Loss resistance 1&2 (r)/Ω	0.8
Loss resistance of receiver (r_S)/Ω	1
Load (R_L)/ Ω	20

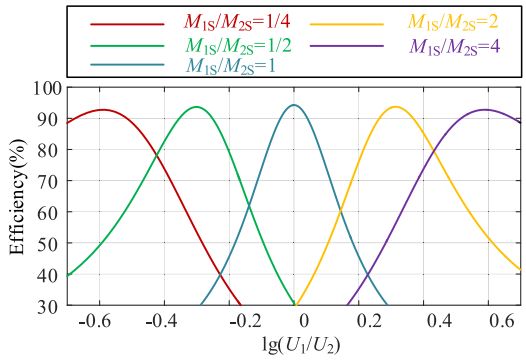

Fig. 4. Efficiency varying with voltage ratio under misalignment condition.

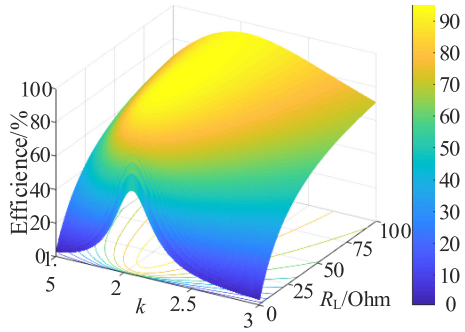

Fig. 5. Efficiency varying with k and the load R_L when $M_{1S}/M_{2S} = 2$.

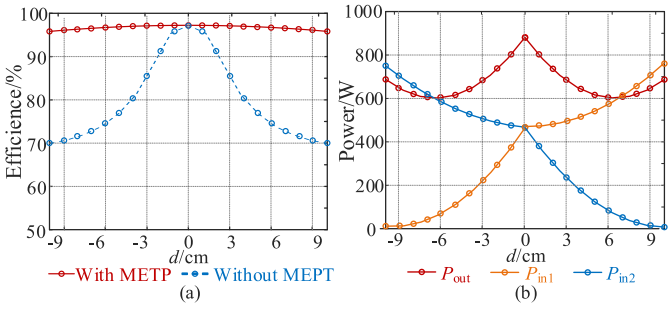

Fig. 6. (a) Maximum efficiency curve of the proposed method and the traditional dual TXs system without any control method. (b) Output and input power variation when the resistance of the load is constant in the proposed system.

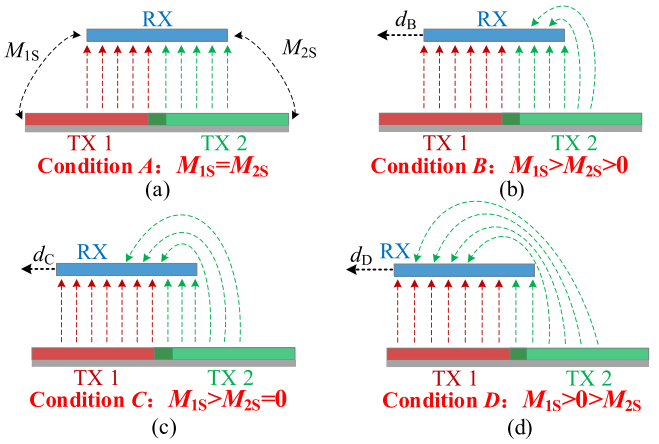

Fig. 7. (a) Transmitting coil and the receiving coil are aligned ($M_{1S} = M_{2S}$). (b) Receiving coil is moving to TX1 horizontally while M_{2S} is positive ($M_{1S} > M_{2S} > 0$). (c) Receiving coil is moving to TX1 horizontally while M_{2S} is zero ($M_{1S} > M_{2S} = 0$). (d) Receiving coil is moving to TX1 horizontally while M_{2S} is negative ($M_{1S} > M_{2S} > 0$).

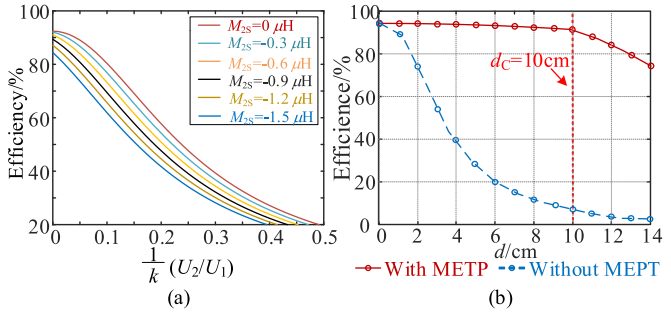

Fig. 8. (a) Efficiency versus voltage ratio under the different values of M_{2S}. (b) Maximum efficiency curve of the proposed method and the traditional dual TXs system without any control method in the redesigned coil structure. When $d > d_C$, the mutual inductance (M_{2S}) is negative.

the equivalent impedance of two TXs are adjusted to equal by MEPT under different position. The proposed system can maintain a higher efficiency utilizing impedance matching. In contrast, the efficiency of such a system without MEPT will be decreased dramatically. The power variation can be obtained as Fig. 6(b), where P_{in1}, P_{in2}, and P_{out} are the input power of TX1, the input power of TX2 and output power, respectively.

B. Tolerance of Misalignment

It is necessary to illustrate misalignment tolerance limitation in a multitransmitter wireless power system, and the event can be analyzed as four conditions, as shown in Fig. 7. The mutual inductance will fluctuate in the process of moving so that the PWM should be adopted to distribute the energy transferred by two TXs which undertake the same energy transmission in condition *A*. The TX1 will work as the main energy transmission channel with RX close to the TX1, as shown in Fig. 7(b). Magnetic lines emitted from TX2 will go to RX from the bottom and the top, respectively. However, the mutual inductance (M_{2S}) will be equal to zero when the magnetic line from the bottom to the RX is equal to that from the top to the RX, as presented in Fig. 7(c). Similarly, M_{2S} will be smaller than zero under condition *D* so that the ratio of mutual inductance (M_{1S}/M_{2S}) is negative. For example, the mutual inductance will be negative if $d > 100$ mm in this system, as shown in Fig. 21. Furthermore, some researchers discuss such situation where the mutual inductance is negative [26], [27], and the work [28] and [29] improve misalignment tolerance for IPT system using such characteristic. The physical mechanism of the negative mutual inductance can be given in Appendix A.

To illustrate this situation better, the efficiency versus voltage ratio ($k = U_1/U_2$) under different values of M_{2S} (0–−1.5μH) are given in Fig. 8(a).

As a result, the efficiency will get the maximum value if U_2 is equal to zero under the condition that $M_{2S} < 0$, and it will drop off dramatically if $1/k$ (U_2/U_1) increases. In other words, the TX2 should be turned OFF under this circumstance. Therefore, it will become the single-TX and single-RX system. Therefore, the tolerance of misalignment of such a method can be summarized as $-d_C \le d \le d_C$. Fig. 8(b) gives the maximum efficiency curve based on the proposed coil structure. The efficiency will drop off dramatically when $d > d_C$.

C. Effect on M12 (Mutual Inductance Between TX1 and TX2)

Generally speaking, the mutual inductance between TX1 and TX2 (M_{12}) will influence the efficiency dramatically. It is necessary to illustrate the relationship between the system's efficiency and M_{12}. The mutual decoupling of the coils constituting the BPP is achieved by adjusting the overlap of the two coils, and the mutual inductance between the two coils depends on the extent of overlap [25].

M_{12} is taken into (20) to study the effect of M_{12} on the transfer efficiency so that the images of efficiency and input conductance versus voltage ratio k are drawn at a different value of M_{12}.

As shown in Fig. 9, the input conductance of TX1 (TX2) will reduce (increase) when the voltage ratio k (U_1/U_2) increases. The input conductance will be equal at point *E,* while the efficiency will get the maximum value at point *F*. In Fig. 9(a), the system will get the maximum efficiency at point *E*. Whereas, the maximum efficiency point will deviate from *E* when the transmitting coils are coupled. And the efficiency will decrease dramatically when coupling strength between two transmitting coils are enhanced.

As a result, if M_{12} is too large to ignore, the system cannot work at the maximum efficiency point using the proposed impedance matching method. As shown in Fig. 10, the red line is the maximum efficiency in theory (Point *F*), and the black line is the maximum efficiency using the proposed impedance matching method (Point *E*) when $M_{1S}/M_{2S} = 2$.

D. Topology and Control Method

The above deduction illustrates that the equivalent conductance of TXs is the same so that the efficiency can get maximum value in a dual TXs system (M_{12} is too small so that it can be ignored).

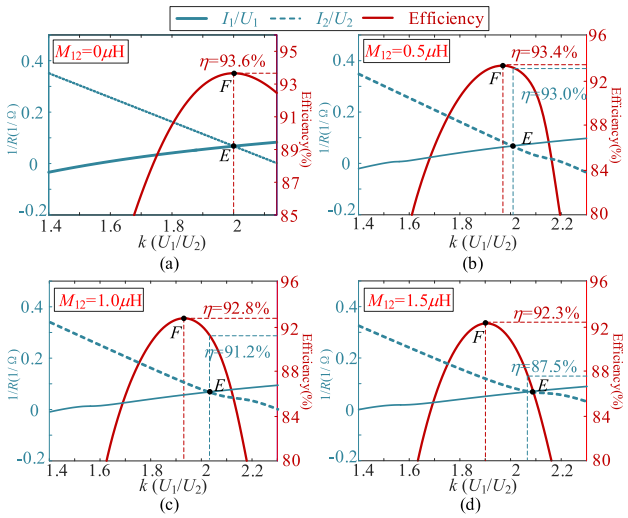

Fig. 9. (a) Efficiency and input conductance of TXs varying with voltage ratio when $M_{12} = 0$ μH and $M_{1S}/M_{2S} = 2$. (b) Efficiency and input conductance of TXs varying with voltage ratio when $M_{12} = 0.5$ μH and $M_{1S}/M_{2S} = 2$. (c) Efficiency and input conductance of TXs varying with voltage ratio when $M_{12} = 1.0$ μH and $M_{1S}/M_{2S} = 2$. (d) Efficiency and input conductance of TXs varying with voltage ratio when $M_{12} = 1.5$ μH and $M_{1S}/M_{2S} = 2$.

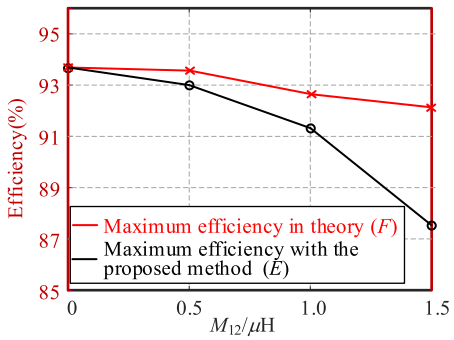

Fig. 10. Maximum efficiency versus M_{12}. The red line presents the maximum efficiency in theory, while the black line presents the efficiency when the input conductance of two TX is equal $(M_{1S}/M_{2S}) = 2$.

As shown in Fig. 11, each TX is driven by a full-bridge inverter, while a boost converter is introduced into the receiver side. L_B, S_B, and D_B are the inductance, the MOSFET, and the diode in the boost circuit, respectively. D_k is the duty cycle of U_k, while θ_k is the conduction angle of the kth inverter. The sequence diagram of the MOSFET of the kth inverter is given in Fig. 12. The relationship between D_k and θ_k can be obtained as follows:

$$\theta_k = D_k \cdot 180^\circ. \tag{21}$$

The equivalent conductance G_k of TX^k is a function against θ_k, which can be defined as follows:

$$G_k = \frac{\pi \cdot I_k}{2V_g \cdot \sin(\theta_k/2)}. \tag{22}$$

R_{AC} and R_{Leq} are the equivalent resistance of the port EF and the port PQ, respectively. D is the duty cycle of the S_B. The work [30] and [31] give the theoretical derivation process of the input

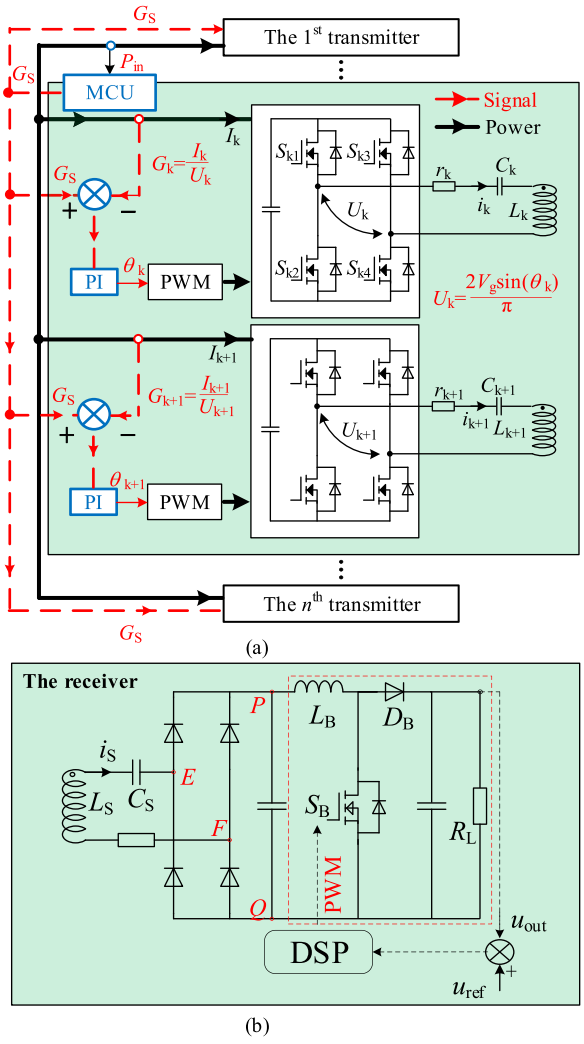

Fig. 11. (a) Diagram of the topology in the multiple-transmitter system. (b) Topology of the RX with a boost converter.

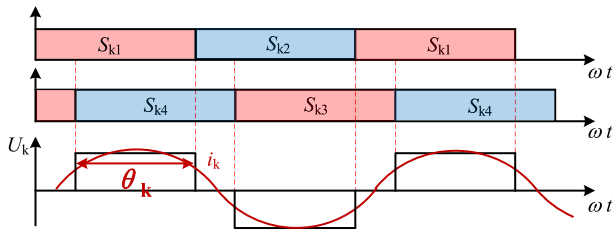

Fig. 12. Sequence diagram of the MOSFET of the kth inverter. θ_k is the angle where S_{k1} and S_{k4} are both on.

impedance in the DCDC converter. Similarly, the relationship of R_{AC}, R_{Leq}, and R_L at continuous conductive mode (CCM) and discontinuous conductive mode (DCM), respectively, can be described as follows:

$$\begin{cases} R_{\mathrm{AC}} = \frac{8}{\pi^2} \cdot R_{\mathrm{Leq}} = \frac{8}{\pi^2} \cdot (1-D)^2 \cdot R_{\mathrm{L}} & \text{CCM} \\ R_{\mathrm{AC}} = \frac{8}{\pi^2} \cdot R_{\mathrm{Leq}} \\ \quad = \frac{4R_{\mathrm{L}}T_{\mathrm{b}}D^2 + 16L_{\mathrm{B}} + 4 \cdot \sqrt{R_{\mathrm{L}}{}^2 T_{\mathrm{b}}{}^2 D^4 + 8L_{\mathrm{B}}R_{\mathrm{L}}}}{\pi^2 T_{\mathrm{b}} D^2} & \text{DCM}. \end{cases} \tag{23}$$

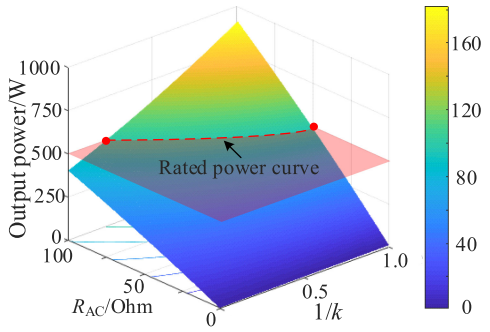

Fig. 13. Output power varying with k and the load R_L when $M_{1S}/M_{2S} = 2$.

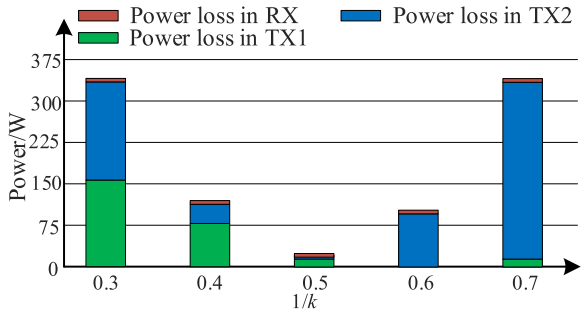

Fig. 15. Comparison of power losses at TX coils and the RX coil with respect to the TX voltage ratio (M_{2S} /$M_{1S} = 0.5$).

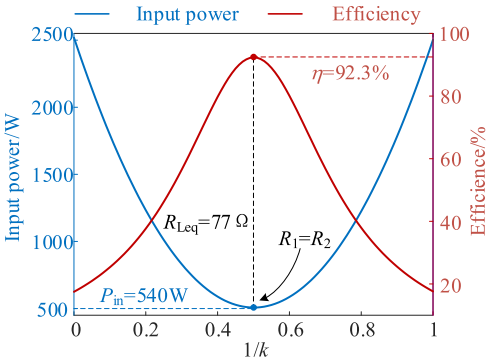

Fig. 14. Efficiency and the input power varying with k under the constant output power mode ($P_{out} = 500$ W, M_{2S} /$M_{1S} = 0.5$).

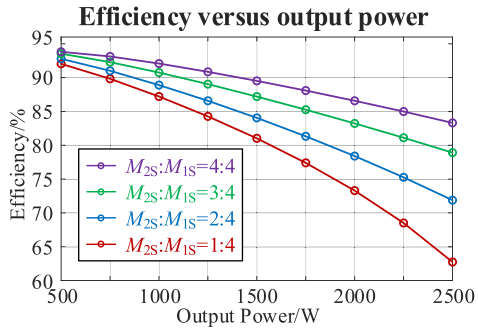

Fig. 16. Maximum efficiency versus the output power level.

The theoretical derivation process can be given in Appendix B. R_{Leq} is the function of D. The output power of such dual TX system can be described as follows:

$$P_{\text{out}} = \dot{i}_S \cdot \overline{\dot{i}_S} \cdot R_{\text{AC}}(D) = \frac{R_{\text{AC}}(D) \cdot \omega^2 \cdot {U_1}^2 \cdot (M_{1S} + M_{2S})^2}{k^2 \cdot \left[r \cdot (r_S + R_{\text{AC}}(D)) + \omega^2 \cdot \left({M_{1S}}^2 + {M_{2S}}^2\right)\right]^2} \tag{24}$$

where $k = U_1/U_2$. The essence of maintaining the constant output power by adjusting the duty cycle of the boost is to adjust the equivalent impedance from the port PQ. Fig. 13 shows the dependence of P_{out} on R_L and k under the condition that $M_{2S}/M_{1S} = 0.5$. Unless otherwise specified, all the theoretical analysis results and figures are based on the parameters listed in Table I.

As shown in Fig. 13, points on the rated power curve own the different value of R_{AC} and k. Taking these points into (24), the input power and efficiency varying with k can be presented as Fig. 14(a). The efficiency has the maximum value, while the input power owns the minimum value when k is equal to the ratio of M_{1S} and M_{2S}. Under this condition, R_{Leq} is equal to 77 Ω by adjusting the duty cycle of boost.

Fig. 15 shows the power loss distribution as a function of the ratio k ($k = U_1/U_2$). As RX moves to TX1, RX and TX2 are weakly coupled so that the current in TX2 (i_2) will increase. The proposed method can adjust the input voltage of TXs to reduce the unnecessary current by changing k.

Fig. 16 gives the relationship between the efficiency and the output power under different misalignment. The maximum efficiency point will drop down when the output power increases.

The control strategy of a multiple-transmitter system based on two decoupled control feedback loops can be designed. The first controller is used to boost to realize constant output power by regulating the equivalent resistance of $R_{Leq}(D)$. Such a control loop has a faster response time to keep the constant output power quickly.

The second control loop, which is the primary controller, is used to achieve impedance matching and find the minimum value of input power (P_{in}) by adjusting θ_{k}. The RX moves toward TX1 horizontally so that $M_{1S} > M_{2S}$. The equivalent input impedance of the kth transmitter can be given in (25), shown at the bottom of this page.

Therefore, the kth input conductance G_k can be reduced (increased) when the voltage of kth transmitter (U_k) is reduced

$$G_k = \frac{I_k}{U_k} = \frac{[r \cdot (r_S + R_{\text{AC}}) + \sum_{j=1, j\neq k}^{j=n} \omega^2 {M_{jS}}^2] - \frac{1}{U_k} \cdot \omega^2 M_{kS} (\sum_{j=1, j\neq k}^{j=n} U_j \cdot M_{jS})}{[r^2 \cdot (r_S + R_{\text{AC}}) + \sum_{j=1}^{j=n} \omega^2 {M_{jS}}^2 \cdot r]} \tag{25}$$

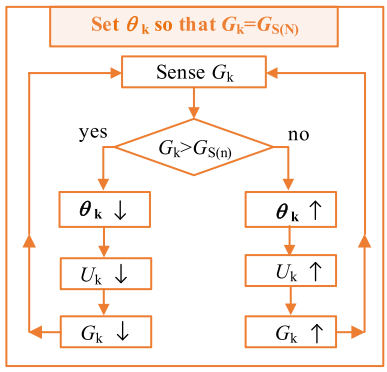

Fig. 17. Input conductance of each Tx is set to be a target value $G_S(N)$, so that all G_k are equalized ($G_1 = G_k = G_n$).

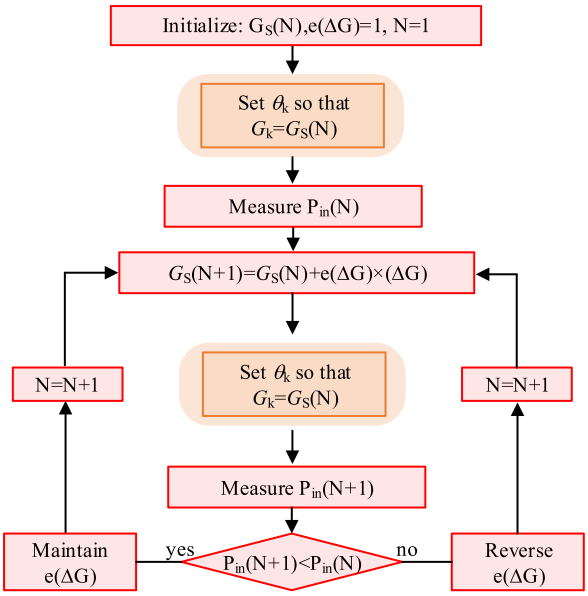

Fig. 18. Overall system optimization procedure. $e(\Delta G)$ is the polarity of ΔG, which is 1 or –1. The P_{in} monitoring is by sensing dc voltage and current at dc supply node.

(increased). It is realized by a PI feedback control within an individual transmitter. Fig. 17 shows that all G_k are enforced to approach a target value, G_{S}. Therefore, the G_k can be controlled by adjusting θ_k. This achieves the first step of control which realizes $G_1 = G_2 = \cdots = G_k$.

According to Fig. 14, there exists the minimum input power when the voltage ratio (k) changes. In other words, there exists an optimum target input conductance (G_S), which can minimize the input power. As shown in Fig. 18, the overall loop searches for an optimum G_S while the voltage ratio setting of Fig. 17 is also performed in each TX. This article mainly discusses the dual-transmitter system in AGV ($n = 2$).

IV. Experiment Results

As shown in Fig. 19, a prototype WPT system is set up to verify the proposed impedance matching method according to the parameters in Table II. f_{s} is the frequency of such a system

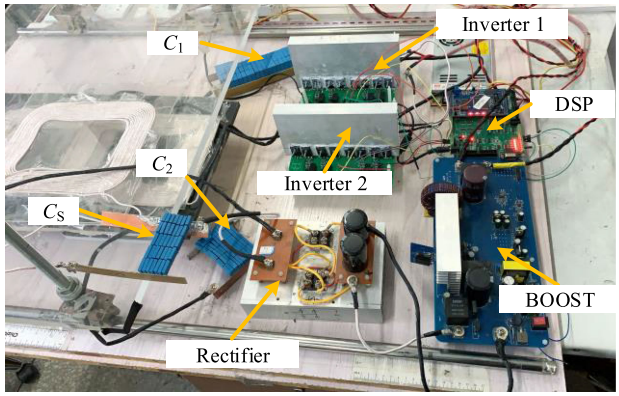

Fig. 19. Experimental setup.

TABLE II
Parameters of the Proposed Method for Experiment

Parameter	Value	Parameter	Value
V_{g}	110 V	N	16
f_{s}	85000 Hz	R_{L}	23 Ω
C_1	29.02 nF	L_1	120.95 μH
C_2	31.32 nF	L_2	111.94 μH
C_{S}	52.1 nF	L_{S}	67.3 μH

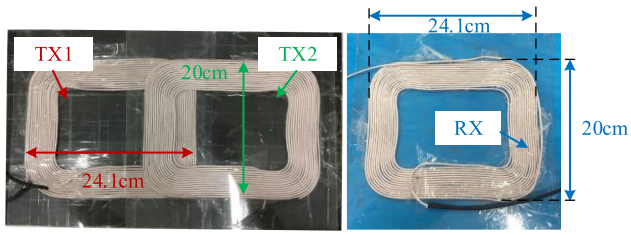

Fig. 20. Size of the transmitter coils and the receiver coil, respectively.

while N is the turns of RX and TXs, which are equal. L_1 (C_1), L_2 (C_2), and L_{S} (C_{S}) are the self-inductance (compensation capacitor) of the transmitting coil one, transmitting coil two, and the receiving coil, respectively. SiC MOSFETS (C2M0160120D) are chosen as the switches in two inverters with a single dc input source (IT6526D) in TX. The gate drives the signal, and the MEPT method with impedance matching is generated by the DSP28335. The single RX coil has connected the rectifier, and an electronic load (IT8818BS) serves as a load resistor. The air gap between the TX and RX is 5 cm, while the TX is covered with ferrite cores.

As shown in Fig. 20, the dimensions of TXs and RX are all 24.1 cm × 20 cm. The coil is wounded by Litz wire of 3 mm × 600 strands.Fig. 21 shows the fluctuation of M_{12}, $M_{1\text{S}}$, and $M_{2\text{S}}$ when the horizontal misalignment occurs, and distance (d) changes from 0 to 14 cm.

The voltage of TX1 can be adjusted by changing θ_{k} when RX is moving toward TX2. The voltage ratio of two TXs can be given as follows:

$$k = \frac{U_1}{U_2} = \frac{\sin(\theta_1/2)}{\sin(\theta_2/2)}. \tag{26}$$

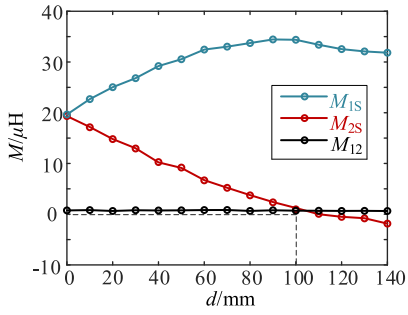

Fig. 21. Mutual inductance of the proposed coupling model under misalignment condition.

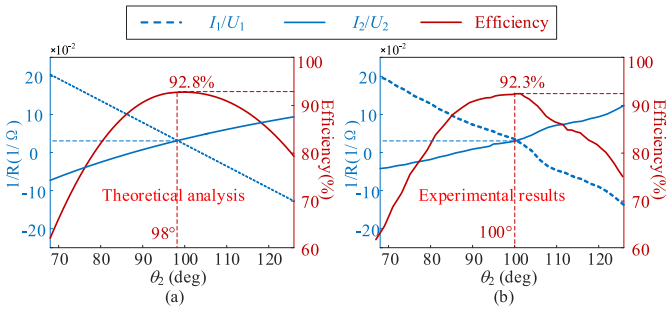

Fig. 22. (a) Equivalent conductance and efficiency versus angle θ_2 in theoretical analysis. (b) Equivalent conductance and efficiency versus angle θ_2 in experimental results. The blue lines represent the equivalent conductance of TX1 and TX2, while the red lines represent the transfer efficiency ($M_{1S}/M_{2S} = 4/3$, $P_{out} = 500$ W).

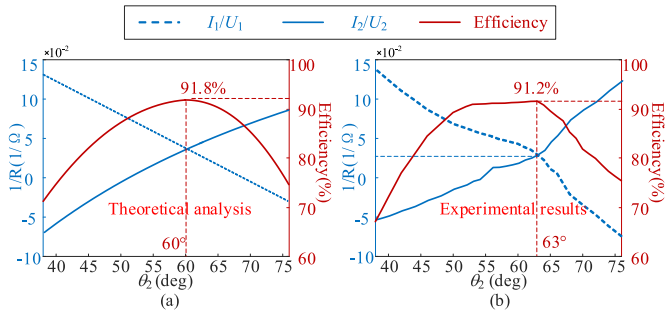

Fig. 23. (a) Equivalent conductance and efficiency versus angle θ_2 in theoretical analysis. (b) Equivalent conductance and efficiency versus angle θ_2 in experimental results. The blue lines represent the equivalent conductance of TX1 and TX2, while the red lines represent the transfer efficiency ($M_{1S}/M_{2S} = 2/1$, $P_{out} = 500$ W).

θ_2 should decrease so that the energy transferred through TX2 will decrease, while TX1 serves as the main channel of energy transmission because of the constant value of θ_1=180°. The voltage ratio of two TXs can be converted into $k = \frac{\sin(180°/2)}{\sin(\theta_2/2)} = \frac{1}{\sin(\theta_2/2)}$. For the convenience of experimental records, the system's efficiency, and the equivalent conductance versus angle θ_2 are shown in Figs. 22 and 23.

In Fig. 22, the voltage ratio will be changed by adjusting θ_2. The ratio of mutual inductance is 4/3, and the voltage ratio (k) should be set to 4/3 so that the equivalent conductance of two

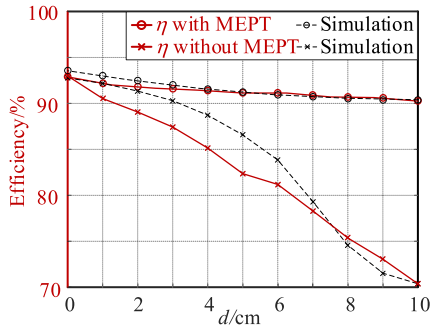

Fig. 24. Efficiency curves of the proposed system with MEPT and without MEPT. The red lines are based on the experiment data, while the black lines are based on the simulation data.

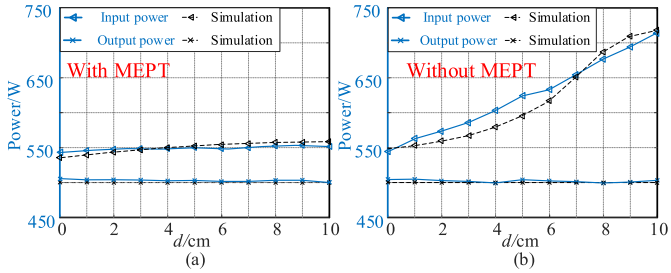

Fig. 25. (a) Output power and input power of the proposed system with MEPT. (b) Output power and input power of the proposed system without MEPT. The red lines are based on the experiment data while the black lines are based on the simulation data.

TXs is equal. In such a condition, the transfer efficiency can get the maximum value. The experiment can be shown in Fig. 22(b), and the value of voltage ratio ($\theta = 100°$, $k = \frac{1}{\sin(\theta_2/2)}$) is 1.305 while the ratio of mutual inductance (M_{1S} / M_{2S}) is 1.33. The experimental results are very close to the theoretical analysis. In both experiment and theoretical analysis, the efficiency will get the maximum value when the equivalent conductance of two TXs are equal.

Similarly, Fig. 23 gives the theoretical analysis and experimental results of equivalent conductance and the efficiency when M_{1S} / M_{2S} = 2/1.

Fig. 24 shows the efficiency curve of the proposed system with MEPT and without MEPT, respectively. The red lines are based on the experiment data, while the black lines are based on the simulation data. Such the MEPT method can maintain a higher efficiency utilizing impedance matching in contrast to that without this method. The efficiency is higher than 90% when the RX moves from 0 to 10 cm.

Fig. 25 gives the output power and the input power of the proposed system with MEPT and without MEPT, respectively. The blue lines are based on the experiment data, while the black lines are based on the simulation data. Such a system can maintain a constant output power utilizing a boost converter in RX with or without the use of MEPT.

Fig. 26 shows the measured ratios of mutual inductance and TX coil currents with respect to the RX position for 10 cm lateral distance separation. The theoretical analysis states that

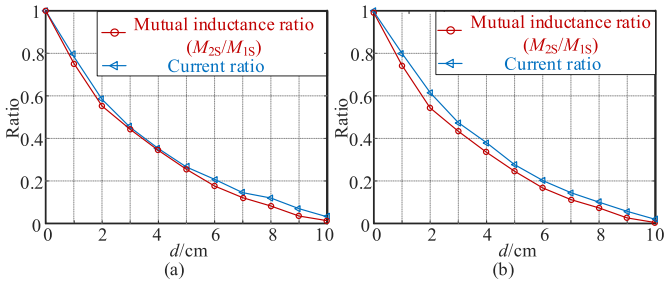

Fig. 26. Measured mutual inductances and TX coil currents for the proposed control method. (a) Output power is 500 W. (b) Output power is 600 W.

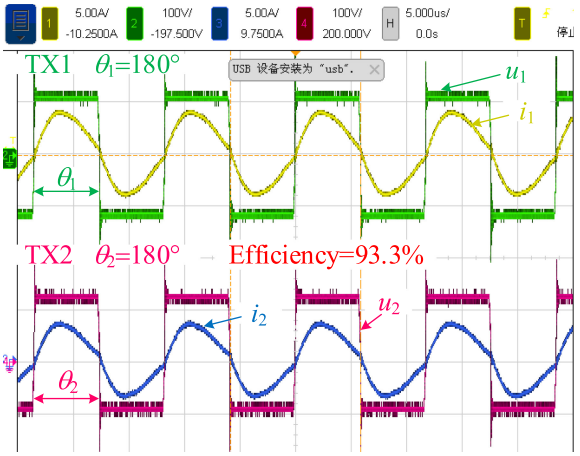

Fig. 27. Experimental waveforms of voltages u_1, u_2, and currents i_1, i_2 when $M_{1S}/M_{2S} = 1$.

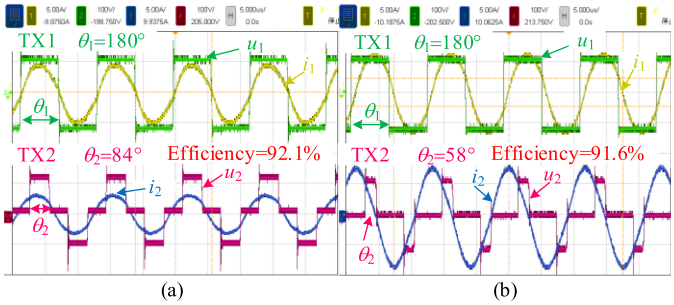

Fig. 28. (a) Experimental waveforms of voltages u_1, u_2, and currents i_1, i_2 when $M_{1S}/M_{2S} = 3/2$. (b) Experimental waveforms of voltages u_1, u_2, and currents i_1, i_2 when $M_{1S}/M_{2S} = 2/1$.

the current ratio and the voltage ratio should be set to the same as the mutual inductance ratio so that MEPT can be realized. It can be seen that the current ratio successfully tracks the mutual inductance ratio using the proposed method.

The experimental waveforms of voltages u_1, u_2, and currents i_1, i_2 are shown in Fig. 27, with the operating conditions of $V_g = 110$ V and $P_{out} = 500$ W when transmitters and the receiver are aligned.

When the RX moves toward the TX1, the voltage of TX2 will decrease so that i_2 will drop down, and the TX1 will serve as the master transmitter. Fig. 28 gives the waveforms when $M_{1S}/M_{2S} = 3/2$ and $M_{1S}/M_{2S} = 2/1$, respectively.

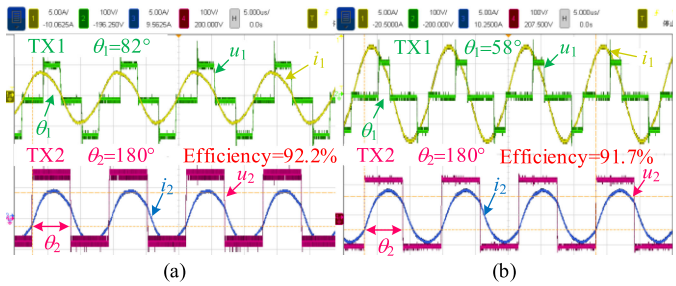

Fig. 29. (a) Experimental waveforms of voltages u_1, u_2, and currents i_1, i_2 when $M_{1S}/M_{2S} = 2/3$. (b) Experimental waveforms of voltages u_1, u_2, and currents i_1, i_2 when $M_{1S}/M_{2S} = 1/2$.

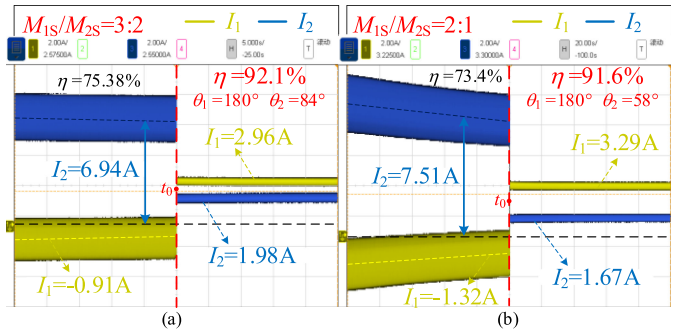

Fig. 30. (a) Input current fluctuation of two inverters in the dual-transmitter system using the proposed MEPT method ($M_{1S}/M_{2S} = 3$:2). (b) Input current fluctuation of two inverters in the dual-transmitter system using the proposed MEPT method ($M_{1S}/M_{2S} = 2$:1).

TABLE III
EQUIVALENT INPUT CONDUCTANCE OF TWO TRANSMITTERS

Condition	M_{1S}/M_{2S}=3:2	M_{1S}/M_{2S}=2:1	Efficiency
G_1 (Before t_0)	-1.299*10^{-2}	-1.885*10^{-2}	75.4% or 73.4%
G_2 (Before t_0)	9.91*10^{-2}	10.724*10^{-2}	
G_1 (After t_0)	4.227*10^{-2}	4.698*10^{-2}	91.6% or 92.1%
G_2 (After t_0)	4.226*10^{-2}	4.919*10^{-2}	

Similarly, the voltage of TX1 will decrease so that i_1 will drop down when the RX moves towards the TX2, and the TX2 will serve as the master transmitter. Fig. 29 gives the waveforms when $M_{1S}/M_{2S} = 2/3$ and $M_{1S}/M_{2S} = 1/2$, respectively.

The input current fluctuation of two inverters in the dual-transmitter system using the proposed MEPT method can be shown as Fig. 30. The efficiency is very low before t_0, while the efficiency is increased dramatically by such a method.

The current ratio after t_0 can be obtained. In Fig. 30(a), $I_1/I_2 = 1.49$, while $M_{1S}/M_{2S} = 1.5$. In Fig. 30(b), $I_1/I_2 = 1.97$, while $M_{1S}/M_{2S} = 2$. The current ratio is roughly equal to the mutual inductance ratio. The equivalent conductance of the kth inverter can be given as follows

$$G_k = \frac{\pi \cdot I_k}{2V_g \sin(\theta_k/2)}. \tag{27}$$

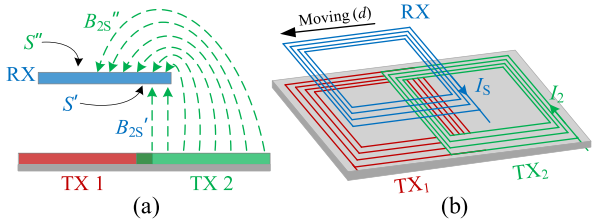

Fig. 31. (a) Distribution of magnetic lines between RX and TX2 when $M_{2S} < 0$. (b) Reference direction of the current direction in TX2 and RX.

The equivalent input conductance of two transmitters can be summarized in Table III, according to Fig. 30. G_1 is roughly equal to G_2 after t_0, and the efficiency is increased dramatically.

V. Conclusion

In this article, an impedance matching method for the multi-TX wireless power system is proposed to realize MEPT under misalignment conditions. According to the theoretical analysis, the efficiency will reach the maximum value if the equivalent impedances of TXs are the same. The equivalent impedance of multi-TX is adjusted at different positions, and efficiency is improved compared to that without such a method. The proposed method is validated by a 500-W experimental prototype. The experimental results show that the efficiency is always higher than 90% with an improvement of 20.3%, and the output power fluctuates very little when the RX moves from 0 to 10 cm (0%–41% of maximum coil size).

Appendix

A. Corresponding Physical Mechanism When the Coupling Coefficient is Negative

It is necessary to illustrate the corresponding physical mechanism when the coupling coefficient is negative, and the work [26] gives the derivation process according to Stokes' theorem. The distribution of magnetic lines of flux between RX and TX2 can be shown in Fig. 31(a), in which the mutual inductance between TX2 and RX is negative. The magnetic lines of flux pass through the receiving coil from the bottom and top, respectively. $B_{2S}{}'$ ($B_{2S}{}''$) is the magnetic field strength at the bottom (top) of the receiving, while S' (S'') is the area of the $B_{2S}{}'$ ($B_{2S}{}''$) on the receiving coil.

The reference direction of the current can be shown in Fig. 31(b). As a result, the magnetic flux of $B_{2S}{}'$ and $B_{2S}{}''$ can be given as follows:

$$\begin{cases} \phi_{2S}{}' = \int_{S'} B_{2S}{}' \mathrm{dS}' \\ \phi_{2S}{}'' = \int_{S''} B_{2S}{}'' \mathrm{dS}''. \end{cases} \tag{28}$$

As a result, the magnetic flux generated by I_2 and passing through the receiving coil can be given as follows:

$$\phi_{2S} = \phi_{2S}{}' - \phi_{2S}{}''. \tag{29}$$

According to Fig. 31(a), $\phi_{2S}{}' < \phi_{2S}{}''$ and the mutual inductance can be given as $M_{2S} = \phi_{2S}/I_2$ [31]. Therefore, M_{2S} will be negative if the position of the receiving coil is shown in Fig. 31(a). Furthermore, when a coupling coefficient is a positive number, it can be considered as inductive coupling. The flow of the system's energy can be shown in Fig. 32(a). P_1 (P_2) is the power that is transferred by TX1 (TX2). However, when the mutual inductance between TX2 and RX (M_{2S}) is negative, the coupling still exists. The energy flow can be shown in Fig. 32(b). TX2 absorbs the energy from RX.

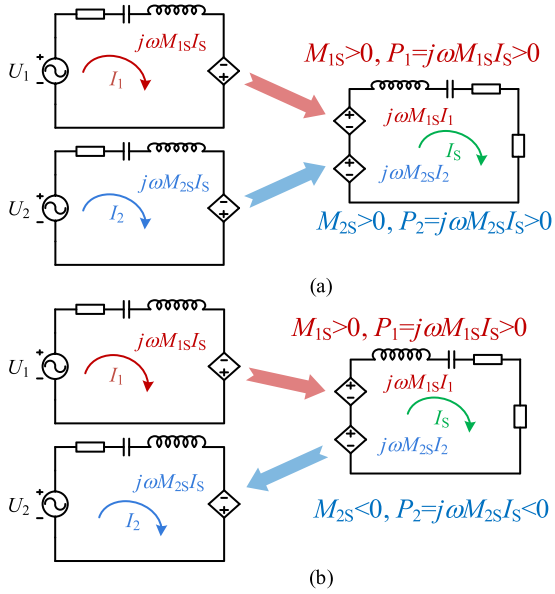

Fig. 32. (a) Energy flow of the two-transmitter system when $M_{1S} > 0$ and $M_{2S} > 0$. (b) Energy flow of the two-transmitter system when $M_{1S} > 0$ and $M_{2S} < 0$.

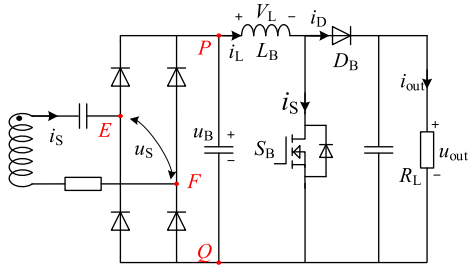

Fig. 33. Topology of the receiver in the proposed multiple-transmitter system.

B. Theoretical Derivation of the Circuit Impedance in Boost

In the proposed system, the boost is used in the RX to make a constant output voltage. As shown in Fig. 33, R_{AC} is the resistance of the port EF, and R_{Leq} is the resistance of the port PQ. R_L is the load. The internal resistance of L_B is ignored.

For the rectifier circuit, the relationship between R_{AC} and R_{Leq} can be easily obtained according to the energy conservation law, which can be expressed as follows:

$$R_{AC} = \frac{8}{\pi^2} \cdot R_{Leq}. \tag{30}$$

Similarly, the relationship between R_{Leq} and R_L of the boost converter can also be obtained according to the energy conservation law assuming there is no power loss in the boost converter.

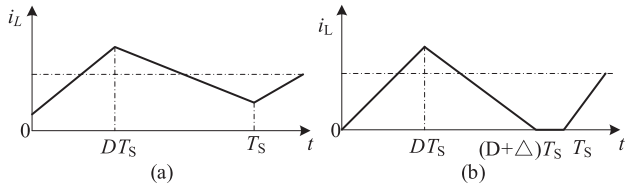

Fig. 34. (a) Waveform of the inductance in boost under CCM condition. (b) Waveform of the inductance in boost under DCM condition.

However, the boost converter can operate at two modes: CCM & DCM, which are determined by whether the inductor current is falling to zero, as shown in Fig. 34.

1) CCM: When the boost converter operates at CCM, the voltage between the inductance is V_{L}, which can be expressed as follows:

$$V_{\mathrm{L}} = \begin{cases} u_{\mathrm{B}} & 0 < t < DT_{\mathrm{S}} \\ u_{\mathrm{B}} - u_{\mathrm{out}} & DT_{\mathrm{S}} < t < T_{\mathrm{S}}. \end{cases} \tag{31}$$

Due to the average voltage of the inductor, the following equation can be derived:

$$\int_0^{DT_S} u_B \, dt + \int_{DT_S}^{T_S} (u_B - u_{\mathrm{out}}) dt = 0. \tag{32}$$

The following equation can be calculated:

$$\frac{u_{\mathrm{out}}}{u_B} = \frac{1}{(1-D)}. \tag{33}$$

According to the energy conservation law, the ratio of the current can be obtained. As a result, the relationship between R_L and $R_{L\mathrm{eq}}$ in CCM can be obtained as follows:

$$R_{L\mathrm{eq}} = (1-D)^2 R_L. \tag{34}$$

2) DCM: Similarly, when the boost converter operates at DCM, the voltage between the inductance can be given as follows:

$$V_L = \begin{cases} u_B 0 < t < DT_S \\ u_B - u_{\mathrm{out}} DT_S < t < (D+\Delta)T_S \\ 0 (D+\Delta)T_{\mathrm{S}} < t < T_S. \end{cases} \tag{35}$$

Due to the average voltage of inductor is zero in one period, we can derive

$$\int_0^{DT_{\mathrm{S}}} u_B \, dt + \int_{DT_S}^{(D+\Delta)T_S} (u_B - u_{\mathrm{out}}) dt = 0. \tag{36}$$

The following equation can be calculated:

$$\frac{u_{\mathrm{out}}}{u_B} = \frac{D+\Delta}{D}. \tag{37}$$

The output voltage when the boost converter operates at DCM can be expressed as follows:

$$u_{\mathrm{out}} = \frac{1 + \sqrt{1 + \frac{2D^2 R_L T_S}{L_B}}}{2} u_B. \tag{38}$$

According to the energy conservation law, the ratio of the current can be obtained. As a result, the relationship between R_L and $R_{L\mathrm{eq}}$ in DCM can be obtained as follows:

$$R_{L\mathrm{eq}} = \frac{2L_B R_L}{L_B + D^2 R_L T_S + \sqrt{{L_B}^2 + 2D^2 R_L T_S L_B}}. \tag{39}$$

In a word, the relationship of R_{AC}, $R_{L\mathrm{eq}}$, and R_L in both CCM and DCM can be given as follows:

$$\begin{cases} R_{\mathrm{AC}} = \frac{8}{\pi^2} \cdot R_{L\mathrm{eq}} = \frac{8}{\pi^2} \cdot (1-D)^2 \cdot R_L & \mathrm{CCM} \\ R_{\mathrm{AC}} = \frac{8}{\pi^2} \cdot R_{L\mathrm{eq}} \\ \quad = \frac{1}{\pi^2} \cdot \frac{16 L_B R_L}{L_B + D^2 R_L T_S + \sqrt{{L_B}^2 + 2D^2 R_L T_S L_B}} & \mathrm{DCM}. \end{cases} \tag{40}$$

REFERENCES

[1] J. M. Miller, O. C. Onar, and M. Chinthavali, "Primary-side power flow control of wireless power transfer for electric vehicle charging," *IEEE J. Emerg. Sel. Topics Power Electron.*, vol. 3, no. 1, pp. 147–162, Mar. 2015.

[2] J. H. Kim *et al.*, "Development of 1-MW inductive power transfer system for a high-speed train," *IEEE Trans. Ind. Electron.*, vol. 62, no. 10, pp. 6242–6250, Mar. 2015.

[3] D. Ahn and S. Hong, "Wireless power transmission with self-regulated output voltage for biomedical implant," *IEEE Trans. Ind. Electron.*, vol. 61, no. 5, pp. 2225–2235, Jul. 2013.

[4] Y. Jang and M. M. Jovanovic, "A contactless electrical energy transmission system for portable-telephone battery chargers," *IEEE Trans. Ind. Electron.*, vol. 3, no. 3, pp. 520–527, Jun. 2003.

[5] C. K. Lee, W. X. Zhong, and S. Y. R. Hui, "Effects of magnetic coupling of non-adjacent resonators on wireless power domino-resonator systems," *IEEE Trans. Power Electron.*, vol. 27, no. 4, pp. 1905–1916, Apr. 2012.

[6] H. Takanashi, Y. Sato, Y. Kaneko, S. Abe, and T. Yasuda, "A large air gap 3 kW wireless power transfer system for electric vehicles," in *Proc. IEEE Energy Convers. Cong. Expo.*, Sep. 2012, pp. 269–274.

[7] W. Zhang, S. C. Wong, C. K. Tse, and Q. Chen, "Design for efficiency optimization and voltage controllability of series–series compensated inductive power transfer systems," *IEEE Trans. Power Electron.*, vol. 29, no. 1, pp. 191–200, Jan. 2014.

[8] R. Huang and B. Zhang, "Frequency, impedance characteristics and HF converters of two-coil and four-coil wireless power transfer," *IEEE J. Emerg. Sel. Topics Power Electron.*, vol. 3, no. 1, pp. 177–183, Mar. 2015.

[9] S. A. Sis and S. Bicakci, "A resonance frequency tracker and source frequency tuner for inductively coupled wireless power transfer systems," in *Proc. 46th Eur. Microw. Conf.*, 2016, pp. 751–754.

[10] D. W. Seo and J. H. Lee, "Frequency-tuning method using the reflection coefficient in a wireless power transfer system," *IEEE Microw. Wireless Compon. Lett.*, vol. 27, no. 11, pp. 959–961, Nov. 2017.

[11] T. Zarifi, K. Moez, and P. Mousavi, "Impedance matching network for ground eliminated open-ended resonant coil structure in distributed wireless power transmission systems," *IET Sci., Meas. Technol.*, vol. 11, no. 7, pp. 856–860, 2017.

[12] Z. Miao, D. Liu, and C. Gong, "Efficiency enhancement for an inductive wireless power transfer system by optimizing the impedance matching networks," *IEEE Trans. Biomed. Circuits Syst.*, vol. 11, no. 5, pp. 1160–1170, Oct. 2017.

[13] M. Filipiak, "Efficiency of wireless power supply in various configurations of coils," in *Proc. 17th Int. Conf. Comput. Problems Elect. Eng.*, 2016, pp. 1–3.

[14] Y. Chen *et al.*, "A hybrid inductive power transfer system with misalignment tolerance using quadruple D quadrature pads," *IEEE Trans. Power Electron.*, to be published, doi: 10.1109/TPEL.2019.2954906.

[15] P. Jayathurathnage, D. M. Vilathgamuwa, S. D. Gregory, and J. F. Fraser, "Effects of adjacent transmitter current for multi-transmitter wireless power transfer," in *Proc. IEEE Southern Power Electron. Conf.*, 2017, pp. 31–35.

[16] W. X. Zhong, X. Liu, and S. Y. R. Hui, "A novel single-layer winding array and receiver coil structure for contactless battery charging systems with free-positioning and localized charging features," *IEEE Trans. Ind. Electron.*, vol. 9, no. 9, pp. 4136–4144, Dec. 2010.

[17] S. A. Mirbozorgi, H. Bahrami, M. Sawan, and B. Gosselin, "A smart multicoil inductively coupled array for wireless power transmission," *IEEE Trans. Ind. Electron.*, vol. 11, no. 11, pp. 6061–6070, Feb. 2014.
[18] X. Shi and J. R. Smith, "Large area wireless power via a planar array of coupled resonators," in *Proc. Int. Workshop Antenna Technol.*, Mar. 2016, pp. 200–203.
[19] M. Kiani and M. Ghovanloo, "A figure-of-merit for designing high-performance inductive power transmission links," *IEEE Trans. Ind. Electron.*, vol. 60, no. 11, pp. 5292–5305, Nov. 2013.
[20] Y. Li, R. Mai, L. Lu, T. Lin, Y. Liu, and Z. He, "Analysis and transmitter currents decomposition based control for multiple overlapped transmitters based WPT systems considering cross couplings," *IEEE Trans. Power Electron.*, vol. 2, no. 2, pp. 1829–1842, Mar. 2018.
[21] B. H. Waters, B. J. Mahoney, V. Ranganathan, and J. R. Smith, "Power delivery and leakage field control using an adaptive phased array wireless power system," *IEEE Trans. Power Electron.*, vol. 30, no. 11, pp. 6298–6309, Feb. 2015.
[22] S. Huh and D. Ahn, "Two-transmitter wireless power transfer with optimal activation and current selection of transmitters," *IEEE Trans. Power Electron.*, vol. 33, no. 6, pp. 4957–4967, Jun. 2018.
[23] X. Zhang, H. Meng, B. Wei, S. Wang, and Q. Yang, "Mutual inductance calculation for coils with misalignment in wireless power transfer," *J. Eng.*, vol. 3, no. 16, pp. 1041–1044, Apr. 2019.
[24] J. Jouya and K. Dina, "Magnetic MIMO: How to charge your phone in your pocket," in *Proc. Int. Conf. Mobile Comput. Netw.*, Sep. 2014, pp. 495–506.
[25] A. Zaheer, G. A. Covic, and D. Kacprzak, "A bipolar pad in a 10-kHz 300-W distributed IPT system for AGV applications," *IEEE Trans. Ind. Electron.*, vol. 61, no. 7, pp. 3288–3301, Sep. 2013.
[26] M. Budhia, J. T. Boys, G. A. Covic, and C. Huang, "Development of a single-sided flux magnetic coupler for electric vehicle IPT charging systems," *IEEE Trans. Ind. Electron.*, vol. 60, no. 1, pp. 318–328, Jan. 2013.
[27] A. Zaheer, G. A. Covic, and D. Kacprzak, "A bipolar pad in a 10-kHz 300-W distributed IPT system for AGV applications," *IEEE Trans. Ind. Electron.*, vol. 61, no. 7, pp. 3288–3301, Jul. 2014.
[28] Y. Chen, R. Mai, Y. Zhang, M. Li, and Z. He, "Improving misalignment tolerance for IPT system using a third-coil," *IEEE Trans. Power Electron.*, vol. 34, no. 4, pp. 3009–3013, Apr. 2019.
[29] R. Mai, B. Yang, Y. Chen, N. Yang, Z. He, and S. Gao, "A misalignment tolerant IPT system with intermediate coils for constant-current output," *IEEE Trans. Power Electron.*, vol. 34, no. 8, pp. 7151–7155, Aug. 2019.
[30] X. Dai, X. Li, Y. Li, and A. P. Hu, "Impedance-matching range extension method for maximum power transfer tracking in IPT system," *IEEE Trans. Power Electron.*, vol. 33, no. 5, pp. 4419–4428, May 2018.
[31] D. Bui, T. M. Mostafa, A. P. Hu, and R. Hattori, "DC-DC converter based impedance matching for maximum power transfer of CPT system with high efficiency," in *Proc. IEEE PELS Workshop Emerg. Technol., Wireless Power Transfer*, 2018, pp. 1–5.

Zhaotian Yan received the B.Sc. degree in electrical engineering and automation in 2018 from the School of Electrical Engineering, Southwest Jiaotong University, Chengdu, China, where he is currently working toward the Ph.D. degree.

His main research interests include wireless power transfer.

Bin Yang, photograph and biography not available at the time of publication.

Huan Liu, photograph and biography not available at the time of publication.

Changxin Chen, photograph and biography not available at the time of publication.

Muhammad Waqas, photograph and biography not available at the time of publication.

Ruikun Mai (Senior Member, IEEE) received the B.Sc. and Ph.D. degrees in electrical engineering from the School of Electrical Engineering, Southwest Jiaotong University, Chengdu, China, in 2004 and 2010, respectively.

He is currently a Professor with the School of Electrical Engineering, Southwest Jiaotong University. His research interests include wireless power transfer and its application in railway systems, and power system stability and control.

Zhengyou He (Senior Member, IEEE) received the B.S. and M.S. degrees from Chongqing University, Chongqing, China, in 1992 and 1995, respectively, and the Ph.D. degree from Southwest Jiaotong University, Chengdu, in 2001.

Since 2002, he has been a Professor with the School of Electrical Engineering, Southwest Jiaotong University. He was a Visiting Scholar with Cornell University, NY, USA, from 2008 to 2009. His research interests include the area of signal processing and information theory and its application in electrical power systems, and the application of wavelet transforms in power systems.